PHILOSOPHICAL TRANSACTIONS OF THE ROYAL SOCIETY A

*Phil. Trans. R. Soc. A* (2006) **364**, 2573–2596
doi:10.1098/rsta.2006.1841
*Published online* 22 August 2006

# Cationic liposome–DNA complexes: from liquid crystal science to gene delivery applications

By Cyrus R. Safinya[1,2,3,*], Kai Ewert[1,2,3], Ayesha Ahmad[1,2,3], Heather M. Evans[1,2,3], Uri Raviv[1,2,3], Daniel J. Needleman[1,2,3], Alison J. Lin[1,2,3], Nelle L. Slack[1,2,3], Cyril George[3] and Charles E. Samuel[3]

[1]*Department of Materials,* [2]*Department of Physics, and* [3]*Molecular, Cellular & Developmental Biology Department, Biomolecular Science & Engineering Programme, University of California, Santa Barbara, CA 93106, USA*

At present, there is an unprecedented level of interest in the properties and structures of complexes consisting of DNA mixed with oppositely charged cationic liposomes (CLs). The interest arises because the complexes mimic natural viruses as chemical carriers of DNA into cells in worldwide human gene therapy clinical trials. However, since our understanding of the mechanisms of action of CL–DNA complexes interacting with cells remains poor, significant additional insights and discoveries will be required before the development of efficient chemical carriers suitable for long-term therapeutic applications. Recent studies describe synchrotron X-ray diffraction, which has revealed the liquid crystalline nature of CL–DNA complexes, and three-dimensional laser-scanning confocal microscopy, which reveals CL–DNA pathways and interactions with cells. The importance of the liquid crystalline structures in biological function is revealed in the application of these modern techniques in combination with functional transfection efficiency measurements, which shows that the mechanism of gene release from complexes in the cell cytoplasm is dependent on their precise liquid crystalline nature and the physical and chemical parameters (for example, the membrane charge density) of the complexes. In §5, we describe some recent new results aimed at developing bionanotube vectors for gene delivery.

**Keywords: cationic liposomes; liquid crystal phases; gene therapy; gene delivery; synchrotron X-ray scattering; transfection efficiency**

## 1. Introduction

The subfield of gene therapy focusing on developing synthetic vectors (carriers) intended for therapeutic applications, in particular, using cationic liposomes (CLs; closed lipid bilayer membrane shells shown in the blow-up in figure 1) as carriers, has recently fundergone a renaissance (Friedmann 1997; Rinehart *et al.* 1997; Miller 1998, 2003; Stopeck *et al.* 1998; Clark & Hersh

* Author for correspondence (safinya@mrl.ucsb.edu).

One contribution of 18 to a Discussion Meeting Issue ‘New directions in liquid crystals’.

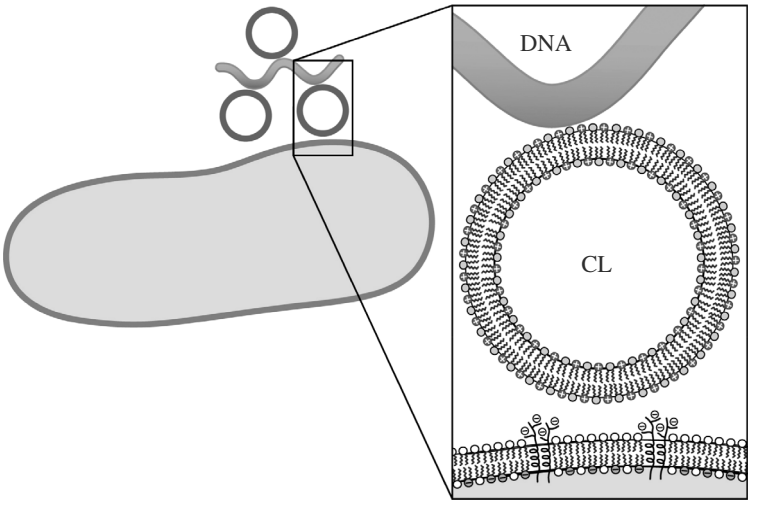


Figure 1. Cartoon of a 'beads-on-a-string' (i.e. CLs attached to a string of DNA) complex electrostatically bound to the surface of an animal cell. The blow-up shows a CL electrostatically binding a section of negatively charged DNA on one side and the plasma membrane containing cell surface proteoglycans with negatively charged sulphated groups on the other side. X-ray diffraction studies have shown that the equilibrium phases of mixtures of CLs and DNA are composed of higher ordered self-assembled liquid crystalline structures, two of which are depicted in figures 2 and 8.

1999; Huang *et al.* 1999, 2005; Chesnoy & Huang 2000; Willard 2000; Ferber 2001; Henry 2001; Niidome & Huang 2002; Mahato & Kim 2002; Safinya *et al.* 2002; Ewert *et al.* 2004, 2005*a*,*b*; Safinya 2001, 2004). To a large extent, this is owing to the non-immunogenicity of synthetic vectors. In addition, with recent technology, the possibility of developing human artificial chromosomes (HACs) containing multiple genes and regulatory constructs for gene therapy applications requires the simultaneous development of the appropriate synthetic carriers for transfer in mammalian cells (Harrington *et al.* 1997; Willard 2000). However, transfection efficiency (TE; a measure of the amount of exogenous DNA transferred into cells followed by gene expression) remains low compared to engineered viral vectors and only a comprehensive knowledge of the interactions between CL–DNA complexes and cells will result in optimization of TE. The long-term objective of research in this area is to develop a fundamental science base, which will lead to a predictive mode for the design and synthesis of optimal synthetic carriers of DNA for gene therapy and disease control.

The first application of CLs as gene vectors resulted from a landmark study by Phillip Felgner and collaborators (Felgner *et al.* 1987; Felgner & Rhodes 1991) and was rapidly followed by numerous pioneering studies by Leaf Huang, which continue to date (Wolff 1994; Huang *et al.* 1999, 2005; Chesnoy & Huang 2000; Niidome & Huang 2002). The original idea shown schematically in figure 1 was that positively charged CL–DNA complexes (with the number of cationic charges from the lipid exceeding the number of negative phosphate groups from DNA) should bind electrostatically to mammalian cells, which contain surface proteoglycans with negatively charged sulphated groups (Mislick & Baldeschwieler 1996;

Mounkes *et al.* 1998). Indeed, the promise of the initial studies showing significant enhancement in cell transfection compared to previous experiments with other synthetic methods led to early clinical trials using CL vectors by Gary and Elizabeth Nabel (Nabel *et al.* 1993), Evan Hersh and collaborators (Rinehart *et al.* 1997; Stopeck *et al.* 1998; Clark & Hersh 1999) and numerous other groups. Presently, more than 20% of the ongoing worldwide human gene therapy clinical trials use synthetic vectors with CL carriers employed in about one-third of those trials (Edelstein *et al.* 2004).

Recent synchrotron X-ray diffraction work has revealed that upon mixing, under equilibrium conditions, CLs (approx. 50–100 nm diameter) and DNA spontaneously self-assemble into novel liquid crystalline phases. Indeed, the beads (CLs)-on-a-string (DNA) model is not observed experimentally. In particular, X-ray studies have led to models of two types of structures observed in CL–DNA complexes. These include a multilamellar structure (labelled $L_{\alpha}^{C}$), shown in figure 2, with DNA monolayers sandwiched between cationic membranes (Lasic *et al.* 1997; Rädler *et al.* 1997, 1998; Salditt *et al.* 1997, 1998; Koltover *et al.* 1999, 2000) and an inverted hexagonal structure with DNA encapsulated within the inverse cylindrical micelles ($H_{II}^{C}$; Koltover *et al.* 1998). Statistical mechanical models have shown that the self-assembled liquid crystalline $L_{\alpha}^{C}$ and $H_{II}^{C}$ phases observed experimentally are indeed equilibrium phases of CL–DNA complexes (Bruinsma 1998; Harries *et al.* 1998; May & Ben-Shaul 2004).

In this paper, we will describe recent work that begins the process of elucidating the relationship between the chemical–physical properties of CL–DNA complexes with well-defined structures (e.g. the membrane charge density and the curvature elastic moduli) and TE in mammalian cells. To achieve these goals, we have used synchrotron X-ray diffraction for structure determination (Rädler *et al.* 1997; Salditt *et al.* 1997; Koltover *et al.* 1998; Lin *et al.* 2003), three-dimensional laser-scanning confocal microscopy (LSCM) to image complex pathways and interactions with cells (Lin *et al.* 2000, 2003) and reporter gene assays to determine TE (Ewert *et al.* 2002; Lin *et al.* 2003; Ahmad *et al.* 2005). The combination of these three characterization methods allows us to rationalize different interactions, observed in confocal microscopy, between high and low TE complexes and cells, based on the knowledge of the structure of the complex. For the lamellar $L_{\alpha}^{C}$ complexes, the data lead to a model with distinct cell transfection regimes for gene delivery as a function of the membrane charge density (Lin *et al.* 2003; Ahmad *et al.* 2005). It is found that the TE behaviour of the inverted hexagonal $H_{II}^{C}$ CL–DNA complexes is independent of the membrane charge density.

All the present methods of gene delivery involve starting with a vector (either an engineered virus or a synthetic carrier), which contains the therapeutic gene followed by either *ex vivo* or *in vivo* transfer methods (Friedmann 1997). In the *ex vivo* method, the vectors mix with and transfect the human cells derived from patient tissue, which are then returned to the patient. The *in vivo* method may involve either systemic delivery, for example, with an injection, or local injections into tumours. In the latter case, most of the current clinical trials are aimed at delivering genes, which encode for cytokines (which are immune cell-signalling molecules), and are expected to result in an immune assault on the tumour (Rinehart *et al.* 1997; Stopeck *et al.* 1998; Clark & Hersh 1999).

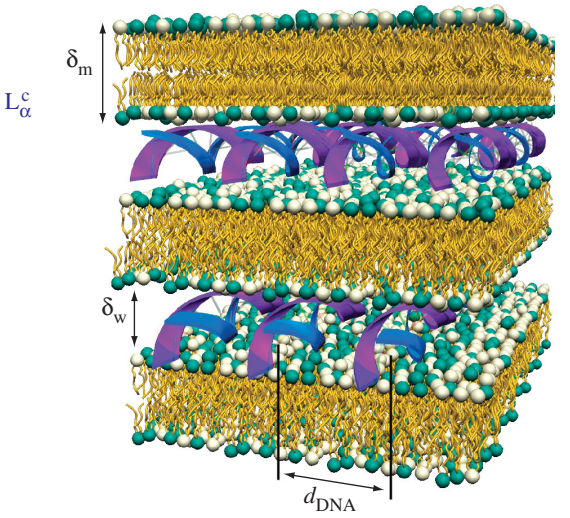


Figure 2. The lamellar $L_\alpha^C$ phase of CL–DNA complexes with alternating lipid bilayer and DNA monolayer. The $L_\alpha^C$ phase is one of the several possible equilibrium phases, which is formed when CLs are mixed with DNA. Redrawn from Rädler *et al.* (1997).

The vectors are divided into two major classes. Viral vectors consist of replication-deficient engineered viruses, which include retroviruses (which integrate within the host chromosome and may offer a permanent cure) and adenoviruses (which do not integrate in the host chromosome and act transiently) among others (Friedmann 1997). Synthetic vectors include carriers consisting of lipids, polymers, designed macromolecules and peptides, or their combinations (Huang *et al.* 1999, 2005; Mahato & Kim 2002; Miller 2003; Safinya 2004).

The main advantage of viral-based vectors is that they have evolved over millions of years to deliver their genome nearly perfectly to their host cells. The viral methods, which started the entire field of gene therapy more than two decades ago, are of course immensely important owing to their extreme high efficiency. However, on occasion, they have also led to undesirable side effects. These include a reported unfortunate death owing to a severe immune response in a trial with engineered adenoviruses (Marshall 2002; Raper *et al.* 2003) and the recent finding of the risk of insertional oncogenesis (incorrect insertion of the therapeutic gene within the regulatory or gene regions of a host genome leading to cancer), where two out of ten children developed leukaemia in a trial to correct X-linked severe combined immunodeficiency with an engineered retrovirus vector (Cavazzana-Calvo *et al.* 2000; Hacein-Bey-Abina *et al.* 2003*a*,*b*; Williams & Baum 2003).

The main problem with synthetic vectors is that they are not yet efficient transfection agents and much more future research and development will be required before their efficiency becomes competitive with viral vectors. On the other hand, they are relatively safe. As mentioned previously, a significant advantage of synthetic vectors is that there is no size limit to the piece of DNA carried by them inside the cells. This was convincingly demonstrated when Willard and Harrington (Harrington *et al.* 1997; Roush 1997; Willard 2000) developed the first HACs, which range in size between six million and ten

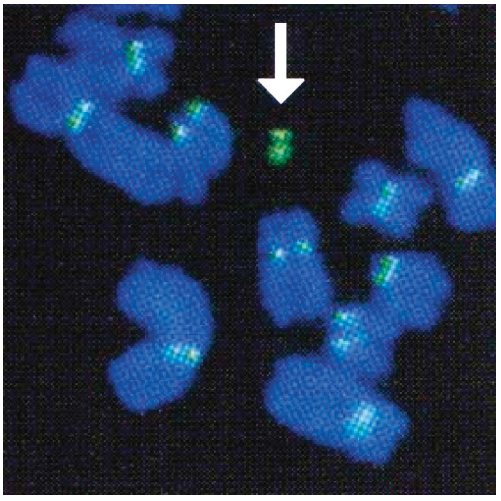

Figure 3. Arrow points to a human artificial chromosome among several normal chromosomes. Adapted from Harrington *et al.* (1997).

million base pairs, about one-tenth of a typical human chromosome (figure 3). (In comparison, viral vectors have a maximum carrying capacity of about 40 000 base pairs. Many important human genes extend over more than 40 000 base pairs, if their regulatory sequences and the non-coding intron regions separating the coding exon sequences are included.) This landmark achievement used CLs as carriers of the HACs into mammalian cells. One can expect that in the future, entire cassettes of genes and regulatory sequences spanning millions of base pairs will be simultaneously delivered for therapeutic applications using synthetic carriers complexed with designer HACs.

The remainder of this paper is organized as follows. After a brief description of the materials in §2, two well-known equilibrium structures of CL–DNA complexes are described in §3. This is followed by a description on the relation between structure and function of CL–DNA complexes and the introduction of some models of cell transfection in §4. Section 5 provides a summary and an outline of future directions in research and development in the vibrant field of synthetic gene delivery. In particular, the section describes the recent work in a new direction focused on developing bionanotubes for gene delivery (Raviv *et al.* 2005). A more detailed accounting of reviews of our group's research (some of which are described in this paper) may be found elsewhere (Safinya 2001; Safinya *et al.* 2002; Ewert *et al.* 2004, 2005*a*,*b*).

## 2. Materials

Selection of lipids used in the studies is shown in figure 4. The charged lipids consisted of univalent cationic dioleoyltrimethylammonium propane (DOTAP) and *N*-(2-hydroxyethyl)-*N*,*N*-dimethyl-2,3-bis(tetradecyloxy)-1-propanaminium (DMRIE), multivalent cationic lipid 2,3-dioleyloxy-*N*-(2-(sperminecarboxamido) ethyl)-*N*,*N*-dimethyl-1-propaniminium penta-hydrochloride (DOSPA) supplied by P. Felgner (then at Vical, Inc.), and a series of custom-synthesized multivalent

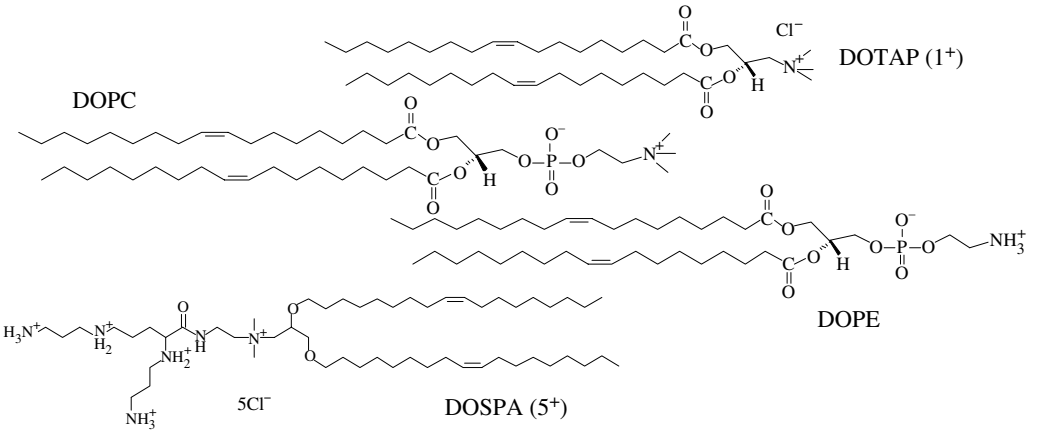


Figure 4. Some lipids used in the structure and function studies of CL–DNA complexes.

headgroup lipids (Ewert *et al.* 2002; Ahmad *et al.* 2005). The neutral lipids consisted of either dioleoyl-phosphatidyl cholin (DOPC) or dioleoyl-phosphatidyl-ethanolamine (DOPE).

The linear DNA consisted of lambda-phage DNA (48 502 bp, contour length = 16.5 μm). Circular plasmid DNA containing the luciferase gene and SV40 promoter/enhancer elements was used for the functional studies (pGL3-control vector, Promega Corporation, Cat. no. E1741). The enzyme luciferase catalyses light production (around 560 nm) in bioluminescent organisms, such as the firefly, jellyfish and some bacteria. The gene from the North American firefly (*Photinus pyralis*) was used for this work. Mouse fibroblast L cell lines were used in the TE studies. The details of the materials and methods are published elsewhere (Koltover *et al.* 1999, 2000; Lin *et al.* 2000, 2003; Ewert *et al.* 2002, 2005*a*,*b*; Ahmad *et al.* 2005).

## 3. Equilibrium structures of cationic liposome–DNA complexes

The mixture of CLs (with an average diameter of approximately 50 nm) with a solution of DNA results in CL–DNA complexes, which are readily observable as well-defined globules using differential interference contrast (DIC) optical microscopy. A series of such images are shown in the micrographs of figure 5 for different weight ratios of total lipid to DNA ($L/D$). The liposomes consisted of a 50/50 wt% mixture of cationic DOTAP and DOPC. The isoelectric point of the CL–DNA complexes occurs at $L/D = 4.4$ for this mixture. At $L/D \approx 5$, the complexes are nearly neutral in charge, and upon colliding, the globules tend to stick owing to the van der Waals attraction leading to large aggregates of globules (figure 5*c*). Polarized microscopy reveals that these aggregates are optically birefringent, which is consistent with their liquid crystalline nature revealed by X-ray diffraction. At $L/D \approx 2$ (figure 5*d*), the complexes are negative and the aggregated globules dissociate owing to electrostatic repulsions. On the other side of the isoelectric point at $L/D \approx 10$ and 50 (figure 5*a*,*b*), the complexes are positively charged and once again the globules tend to repel each other upon approach owing to the electrostatic repulsions.

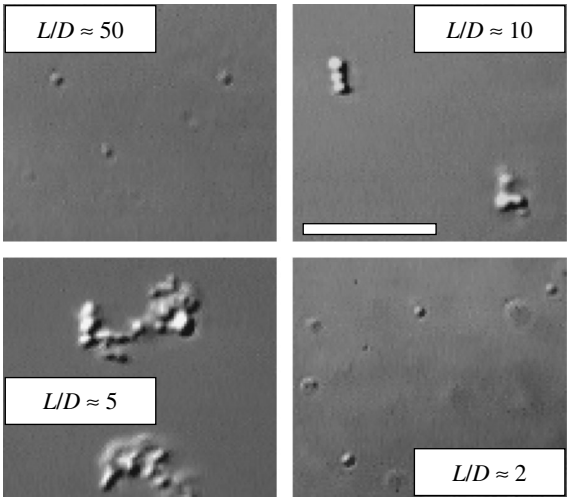


Figure 5. DIC optical micrographs of CL–DNA complexes at different ratios of lipid to DNA ($L/D$) weight ratios. For $L/D>4.4$, the globules are positively charged, and for $L/D<4.4$, the globules are negatively charged. The formation of well-defined globules upon mixing CLs with DNA is readily observable. Scale bar, 10 μm. Adapted from Rädler *et al.* (1997).

Synchrotron X-ray diffraction was used to elucidate the structure of CL–DNA complexes at the angstrom scale. Figure 6 shows synchrotron X-ray diffraction data (taken at the Stanford Synchrotron Radiation Laboratory) of CL–DNA complexes at the isoelectric point (DOTAP/DNA = 2.2, wt/wt) for CLs consisting of a mixture of DOTAP and DOPC (DOPC/DOTAP = 2.2, wt/wt). The sharp 00L peaks, which include the 001 and 002, are visible in this $q$-range. The 003 is absent owing to the form factor and several higher order peaks (not shown) are visible up to 005. The 00L peaks result from the layered structure of the lamellar $L_\alpha^C$ phase of CL–DNA complexes shown in figure 2 with $d=2\pi/q_{001}=\delta_m+\delta_w=64$ Å. $\delta_m=39$ Å is the membrane thickness, which can be measured with X-ray diffraction of the multilamellar lipids in the absence of DNA. The remaining water layer thickness $\delta_w=d-\delta_m=25$ Å is the thickness required to allow a monolayer of DNA in its hydrated B-form sandwiched between the lipid bilayers as shown in figure 2. The broad peak visible between the 001 and 002 corresponds to the DNA–DNA correlation peak and gives an average DNA inter-helical distance of $d_{DNA}=2\pi/q_{DNA}=47.5$ Å for the sample preparation of isoelectric complexes with $L/D=7$. As previously described (Rädler *et al.* 1997; Salditt *et al.* 1997; Koltover *et al.* 1999, 2000), the sandwiched DNA forms a one-dimensional array of chains, which uniformly cover the available lipid area and $d_{DNA}$ is a simple function of $L/D$ and may range from approximately 25 Å ($L/D=2.2$) at high membrane charge densities, where the DNA rods are nearly touching, to as large as about 55 Å ($L/D\approx 9$) at low membrane charge densities. The lamellar $L_\alpha^C$ phase of CL–DNA complexes is a novel hybrid liquid crystalline phase: the lipids form a three-dimensional smectic phase, while the DNA rods between the lipid bilayers form a two-dimensional smectic phase.

The spontaneous self-assembly of CLs and DNA into the lamellar $L_\alpha^C$ phase shown in figure 2 may be understood as follows. In solution, the bare length ($l_o$) between negative phosphate groups on the DNA backbone is equal to 1.7 Å, which is

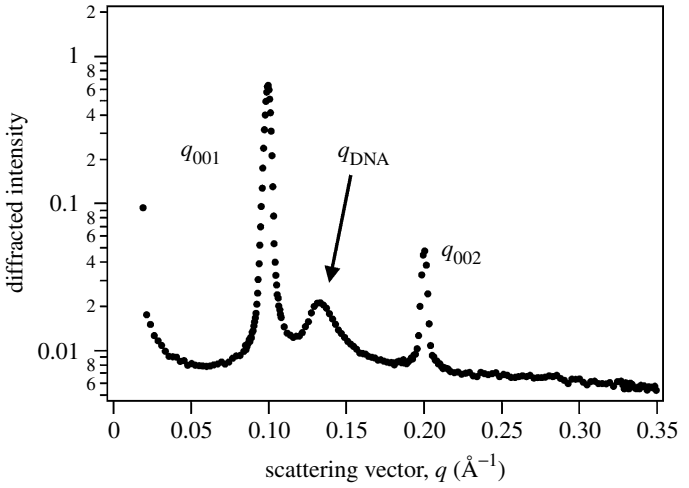


Figure 6. Synchrotron X-ray diffraction pattern of CL–DNA complexes, where the membranes consist of mixtures of cationic DOTAP and the charge neutral lipid DOPC (with a zero spontaneous curvature) with DOTAP/DNA = 2.2 (wt/wt, isoelectric complexes) and DOPC/DOTAP = 2.2 (wt/wt). As described in the text, this diffraction pattern is consistent with the angstrom scale model of the $L_\alpha^C$ phase of CL–DNA complexes shown in figure 2. Adapted from Rädler *et al.* (1997).

less than the Bjerrum length in water, $l_B$ ($\equiv e^2/\varepsilon_w k_B T$) = 7.1 Å (the dielectric constant $\varepsilon_w = 80$). (The Bjerrum length corresponds to the distance where the Coulomb energy between two unit charges is equal to the thermal energy $k_B T$.) Under these conditions, a mean-field nonlinear Poisson–Boltzmann analysis shows that positive counter-ions will condense on the DNA backbone until the Manning parameter $\xi = l_B/l_o^*$ approaches 1 (Manning 1978). Here, $l_o^*$ is the renormalized distance between negative charges after counter-ion condensation. The counter-ion condensation on the DNA backbone is shown schematically in figure 7 (top left).

A similar analysis shown schematically in figure 7 (top right) shows that near the surface of a positively charged membrane (i.e. the CL surface), nearly half of the negative counter-ions are present within the Gouy–Chapman length $l_{G-C} \equiv e/2\pi l_B \sigma$ ($\sigma$ is the charge per unit area of the membrane; Le Bret & Zimm 1984). Through DNA–lipid condensation, the cationic lipid tends to completely neutralize the phosphate groups on the DNA in effect replacing and releasing the originally condensed counter-ions in solution (figure 7, bottom). Thus, the driving force for higher order self-assembly into the lamellar $L_\alpha^C$ phase is the entropy gain through the release of counter-ions, which were one-dimensionally bound to DNA and two-dimensionally bound to cationic membranes, into solution (Rädler *et al.* 1997). We point out that we are using the word 'bound counter-ions' in a very loose form: the bound counter-ions near the macromolecular surfaces are nevertheless in a completely hydrated state and so there is no change in the entropy of water molecules when 'bound counter-ions' are released into solution.

In contrast to the so far discussed neutral lipid DOPC, which confers a zero spontaneous curvature to membranes, another commonly used neutral lipid in CL–DNA mixtures is DOPE. It is well known that DOPE is a cone-shaped lipid, which confers a negative curvature to membranes. Synchrotron X-ray diffraction

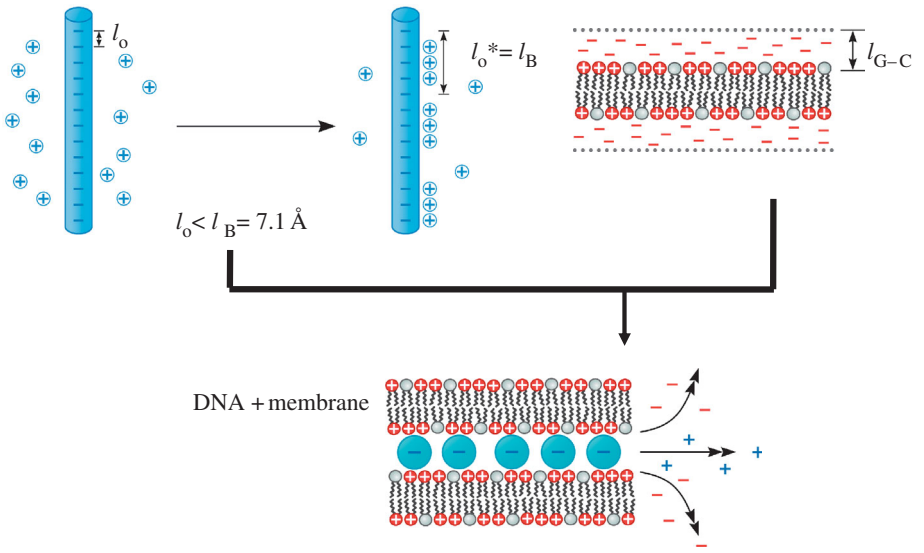


Figure 7. Both DNA and cationic membranes of liposomes (top) have counter-ions 'loosely' bound in the vicinity of their surfaces as described in the text. The DNA–lipid condensation (bottom), which occurs during the formation of the $L_\alpha^C$ phase of CL–DNA complexes can occur as a result of the release of 'bound' counter-ions in solution with a corresponding gain in entropy.

has revealed that mixtures of CLs, which contain DOTAP and DOPE complexed with DNA, may give rise to a completely different columnar inverted hexagonal $H_{II}^C$ liquid crystalline structure shown in figure 8, when the weight fraction of DOPE ($\Phi_{DOPE} \equiv \text{weight}_{DOPE}/(\text{weight}_{DOPE} + \text{weight}_{DOTAP})$) is greater than approximately 0.65 (Koltover *et al.* 1998; Lin *et al.* 2003). The $H_{II}^C$ phase consists of an inverted hexagonal structure, where the DNA molecules are inserted in tubes composed of inverse lipid micelles and assembled on a hexagonal lattice. The structure resembles the inverted hexagonal $H_{II}$ phase of DOPE in excess water (Seddon 1990), with the space inside the micelle filled by DNA.

We can understand the $L_\alpha^C$ to $H_{II}^C$ transition as a function of increasing $\Phi_{DOPE}$ by noting that the spontaneous curvature of the monolayer mixture of DOTAP and DOPE is driven negative with the addition of DOPE: $C_o = 1/R_o = \Phi_{DOPE} C_o^{DOPE}$. Hence, as $\Phi_{DOPE}$ increases, we expect a transition from the $L_\alpha^C$ to the $H_{II}^C$ phase, which is observed experimentally and is favoured by the elastic free energy. Thus, the lipid DOPE induces the $L_\alpha^C$ to $H_{II}^C$ transition by controlling the spontaneous curvature of the membranes.

## 4. Structure–function studies

A major goal in the field of gene delivery with synthetic vectors is the elucidation of the relationship between the structure and the physical–chemical properties of CL–DNA complexes, and their TE (i.e. the function of the complex). For example, it had been known empirically that TE in mammalian cells is significantly higher in CL–DNA complexes, which contain about 70 wt% neutral

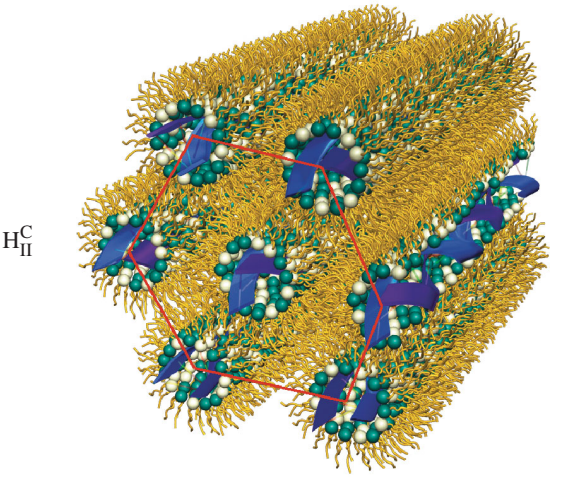


Figure 8. The inverted hexagonal $H_{II}^{C}$ liquid crystalline phase of CL–DNA complexes with DNA chains coated with inverse micelles arranged on a hexagonal lattice. The $H_{II}^{C}$ is one of the several possible equilibrium phases of CL–DNA complexes. Adapted from Koltover *et al.* (1998).

DOPE lipids instead of DOPC (Farhood *et al.* 1995; Hui *et al.* 1996). X-ray diffraction shows that DOTAP containing complexes with 70% DOPE are typically in the $H_{II}^{C}$ phase (Koltover *et al.* 1998; Lin *et al.* 2003). This raises the question of why does the $H_{II}^{C}$ phase transfect better than the $L_{\alpha}^{C}$ phase? The answer is rather subtle: while it is true that CLs with 70% DOPE transfect significantly better than CLs with 70% DOPC (for complexes with univalent cationic lipids), in fact, as we show subsequently, one may design lamellar $L_{\alpha}^{C}$ complexes, which are as transfecting as $H_{II}^{C}$ complexes (Ewert *et al.* 2002; Lin *et al.* 2003; Ahmad *et al.* 2005).

LSCM has been used to shed light on structure–function correlations by directly visualizing, *in three dimensions*, CL–DNA complexes interacting with cells (Lin *et al.* 2003). LSCM provides a spatial resolution of about 300 nm in the $x$- and $y$-directions and 800 nm in the $z$-directions, and allows an unprecedented insight into the mechanisms by which the liquid crystalline complexes enter cells and the conditions that lead to the subsequent release of their cargo DNA molecules. In the experiments, the lipids were labelled with 0.2 wt% Texas Red 1,2-dihexadecanoyl-sn-glycero-3-phosphoethanolamine, triethylammonium salt (DHPE) from Molecular Probes, Inc., which emits red fluorescence at 583 nm, and the DNA was covalently labelled with Mirus Label IT using the PanVera Corporation protocol, which emits green fluorescence at 492 nm. Thus, an intact complex appears yellow.

Figure 9 shows a representative confocal image of a fixed mouse fibroblast L-cell transfected with $H_{II}^{C}$ complexes at $\Phi_{DOPE}=0.69$. (The complexes were allowed to incubate with the cell for 6 h before cell fixation was performed.) The figure shows images from three relevant planes ($x$–$y$, $y$–$z$ and $x$–$z$), which allows one to track the position of the objects within the cell. The lipid fluorescence clearly outlines the plasma membrane, indicating either spontaneous transfer of labelled lipid or fusion of lipids from the membranes of the complex with the plasma membrane before or after entry through the endocytic pathway.

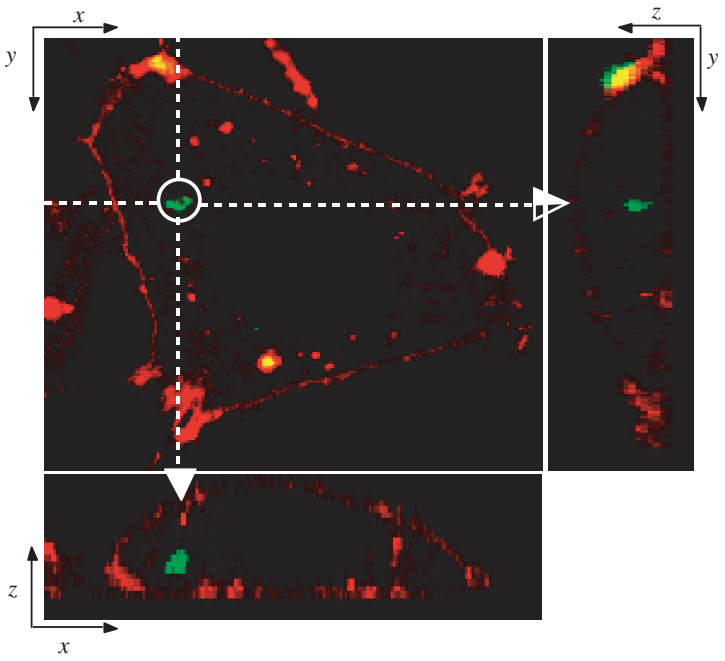


Figure 9. Laser scanning confocal microscopic image of $H_{II}^{C}$ CL–DNA complexes interacting with a mouse fibroblast cell and fixed after 6 h (69 wt% DOPE/31 wt% DOTAP, DOTAP/DNA charge ratio = 2.8). DNA is labelled green and lipid is labelled red. The plasma membrane is seen to be red, which indicates either a direct or indirect fusion event (during endocytosis) with the membrane of complexes as described in the text. The circle in the $x$–$y$ plane identifies a condensed DNA globule, which can also be seen in the $x$–$z$ and $y$–$z$ planes (arrows). Adapted from Lin *et al.* (2003).

Significantly, a condensed piece of DNA (green) may be seen in the cytoplasm. The simplest interpretation of the image is that the interaction between $H_{II}^{C}$ complexes and cells leads to lipid fusion events, which aid in the dissociation and release of DNA from the CL vector. This is also consistent with the known high TE of $H_{II}^{C}$ CL–DNA complexes (Lin *et al.* 2003).

Figure 10 shows similar confocal images of mouse L-cells taken 6 h after incubation with $L_{\alpha}^{C}$ complexes at $\Phi_{DOPC} = 0.67$ to allow optimal transfection. When comparing to figure 9 showing the interaction of $H_{II}^{C}$ complexes with cells, we see no evidence of lipid-free DNA (green), but instead intact CL–DNA complexes are observed inside cells. (Other $x$–$y$ planes at different $z$-positions, not shown here, show the presence of many yellow complexes and no free DNA.) From the image, which does not display any evidence of fusion with the plasma membrane, it is clear that $L_{\alpha}^{C}$ complexes enter cells through endocytosis. Furthermore, when endocytosis is inhibited by preparing cells at 4°C, no complexes are observed inside cells and all remain attached to the cell surface. This observation is consistent with the work of other groups (Wrobel & Collins 1995). Using the reagent chloroquine (which disrupts endosomes), it has been shown that the intact CL–DNA complexes observed in figure 10 are typically trapped within the endosomes (Lin *et al.* 2003). Thus, together with the chloroquine experiments, the confocal image suggests that at $\Phi_{DOPC} = 0.67$, most of the DNA remains trapped by the CL vector within endosomes consistent with the measured low TE.

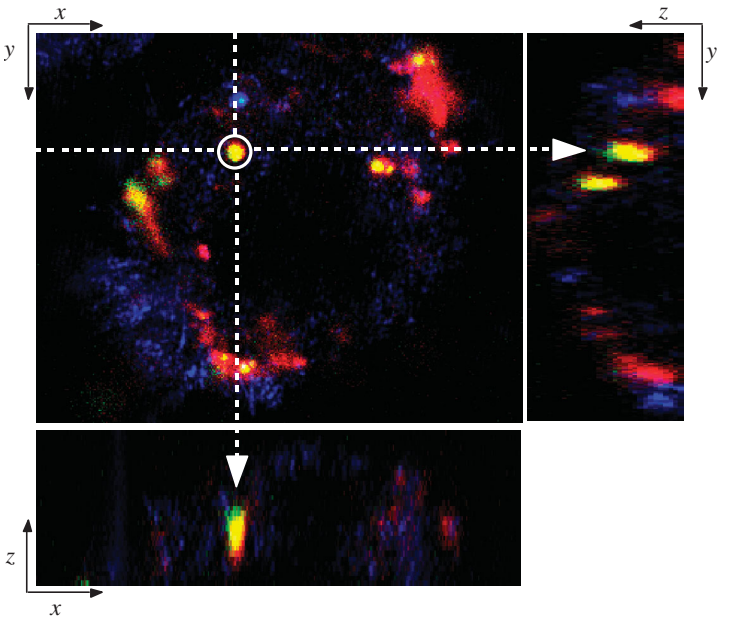


Figure 10. Laser-scanning confocal microscopic image of $L_{\alpha}^{C}$ CL–DNA complexes interacting with a mouse fibroblast L-cell and fixed after 6 h (67 wt% DOPC/33 wt% DOTAP, DOTAP/DNA charge ratio = 2.8). DNA is labelled green and lipid is labelled red. In contrast to figure 9, no fusion with the plasma membrane is seen. Inside the cell, only intact complexes (yellow) are found (circle in $x$–$y$ plane and corresponding arrows in the $x$–$z$ and $y$–$z$ planes). This indicates that for the high weight fraction (0.67) of the neutral lipid DOPC, the CL vector does not release DNA consistent with the observed low TE. Adapted from Lin *et al.* (2003).

To better understand the TE properties of lamellar $L_{\alpha}^{C}$ CL–DNA complexes containing DOPC, an initial study was carried out as a function of mole fractions of DOPC in three commonly available cationic lipids: univalent DOTAP, DMRIE and the multivalent DOSPA ($5^{+}$). The data in figure 11*a* show the increase in TE of DOPC/DOTAP–DNA complexes (red diamonds), which is very low at $0.5 < \Phi_{\mathrm{DOPC}} < 0.7$ and increases substantially in two decades to $\Phi_{\mathrm{DOPC}} = 0.2$, similar to TE of $H_{II}^{C}$ DOPE/DOTAP–DNA complexes. Similar results were obtained for another univalent cationic lipid DMRIE (black triangles). The multivalent cationic lipid DOSPA (blue squares) exhibited strikingly different behaviour, where it was observed that DOSPA containing complexes remained highly transfectant at much larger mole fractions of DOPC, even as large as 0.7 (the point at which the univalent cationic lipids exhibit TE lower in nearly two decades).

The main difference between the cationic lipids is the much higher charge density of DOSPA (see figure 4), with a larger headgroup carrying potentially up to five cationic charges. This implies that for a given $\Phi_{\mathrm{DOPC}}$, the membrane charge density ($\sigma_{\mathrm{M}}$, cationic charge per unit area) is significantly higher in DOSPA compared to DOTAP- or DMRIE-containing complexes. The same TE data are plotted in figure 11*b*, but now versus $\sigma_{\mathrm{M}}$,

$$\sigma_{\mathrm{M}} \equiv [1 - \Phi_{\mathrm{nl}}/(\Phi_{\mathrm{nl}} + r\Phi_{\mathrm{cl}})]\sigma_{\mathrm{cl}}. \tag{4.1}$$

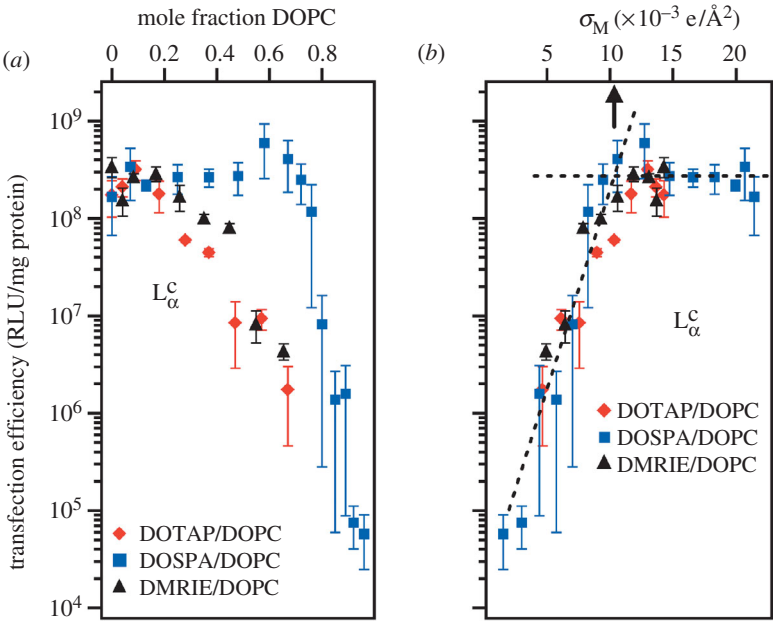


Figure 11. Plots of TE measurements (relative light units normalized to milligrams of protein) in DOPC containing $L_\alpha^C$ CL–DNA complexes. The data are for two univalent cationic lipids (DOTAP and DMRIE) and the multivalent ($5^+$) cationic lipid DOSPA. (*a*) TE versus mole fraction of DOPC. (*b*) Same data as in (*a*), where the TE is plotted versus the membrane charge density of the CL vectors ($\sigma_M$, cationic charge per unit area). Adapted from Lin *et al.* (2003).

Here, $r = A_{cl}/A_{nl}$ is the ratio of the headgroup area of the cationic to neutral lipid, $\sigma_{cl} = eZ/A_{cl}$ the charge density of the cationic lipid with valence $Z$, and $\Phi_{nl} = N_{nl}/(N_{nl} + N_{cl})$ and $\Phi_{cl} = N_{cl}/(N_{nl} + N_{cl})$ the mole fractions of the neutral and cationic lipids, respectively. From the data in figure 11*b*, $A_{nl} = 70$ Å$^2$, $r_{DOTAP} = r_{DMRIE} = 1$, $r_{DOSPA} = 2$, $Z_{DOTAP} = Z_{DMRIE} = 1$ and $Z_{DOSPA} = 3$ (Lin *et al.* 2003).

The data, which are widely spread when plotted as a function of the mole fraction of the neutral lipid (figure 11*a*), collapse onto a universal curve as a function of $\sigma_M$ with TE varying over nearly four decades, while $\sigma_M$ increases by only a factor of approximately 8 ($\sigma_M$ between 0.0015 and 0.012 e Å$^{-2}$). Thus, even though the CL–DNA cell system is very complex, the data show that $\sigma_M$ is a universal parameter for transfection with lamellar $L_\alpha^C$ CL vectors.

To further study the dependence of TE on $\sigma_M$ and access even higher charge densities (compared to the data of figure 11), a novel set of multivalent lipids (MVLs) were synthesized, which allows systematic variation of headgroup size and charge (Ewert *et al.* 2002; Ahmad *et al.* 2005). Figure 12 shows the chemical structure and maximum charge of the MVLs used in this study (Ewert *et al.* 2002; Ahmad *et al.* 2005).

X-ray diffraction shows that the MVLs shown in figure 12 form DNA complexes that exhibit the lamellar ($L_\alpha^C$) phase, the more prevalent of the two known complex structures. Figure 13 shows the TE data plotted versus the membrane charge density for four of the MVL–DNA complexes with charge variation between $2^+$ and $5^+$. To calculate $\sigma_m$, equation (4.1) was used with

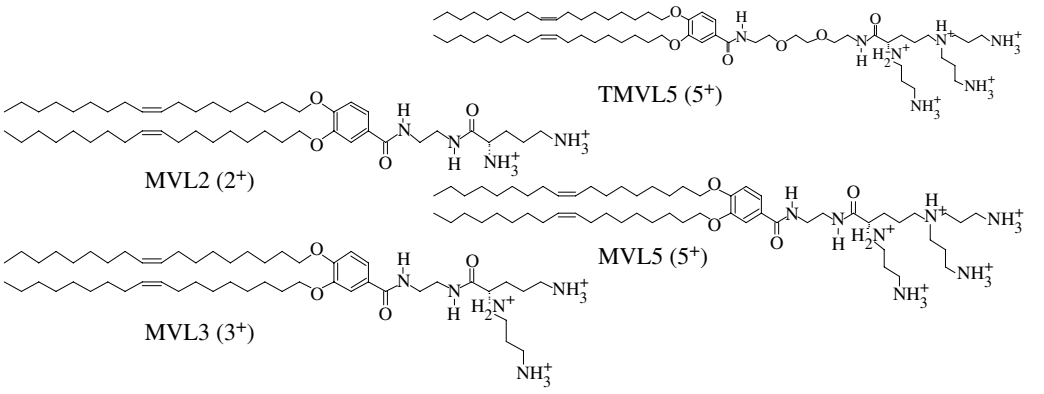


Figure 12. Multivalent cationic lipids specifically synthesized for systematic variation of lipid headgroup size and charge.

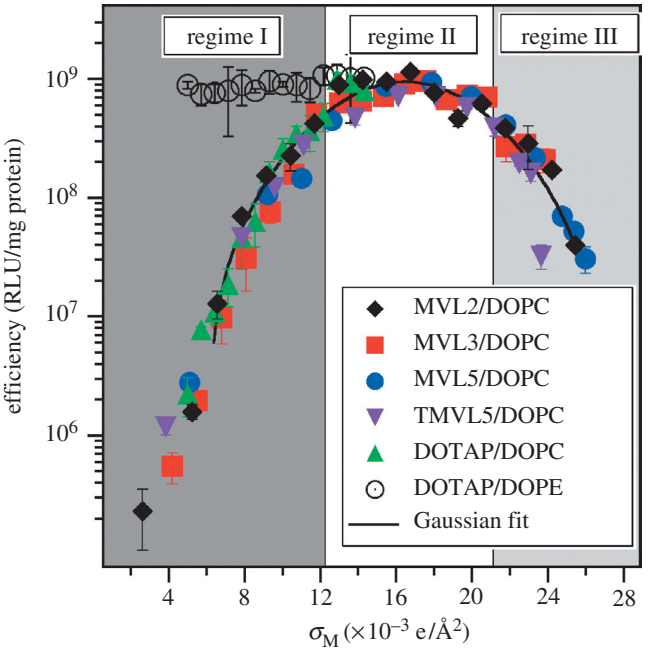


Figure 13. Plots of TE measurements (relative light units normalized to milligrams of protein) versus the membrane charge density ($\sigma_M$) in five DOPC containing $L_\alpha^C$ CL–DNA complexes and contrasted against DOPE containing $H_{II}^C$ CL–DNA complexes (open circle). The $L_\alpha^C$ TE data are for four multivalent cationic lipids (MVL2, MVL3, MVL5 and TMVL5) and the univalent DOTAP. All $L_\alpha^C$ complexes follow a universal curve (consistent with the data of figure 11*b*) for TE versus $\sigma_M$ with a central part that exhibits a bell curve (solid line). Adapted from Ahmad *et al.* (2005).

$A_{nl}=72$ Å$^2$, $r_{DOTAP}=1$, $r_{MVL2}=1.05\pm0.05$, $r_{MVL3}=1.30\pm0.05$, $r_{MVL5}=2.3\pm0.1$, $r_{TMVL5}=2.5\pm0.1$, $Z_{DOTAP}=1$, $Z_{MVL2}=2.0\pm0.1$, $Z_{MVL3}=2.5\pm0.1$ and $Z_{MVL5}=Z_{TMVL5}=4.5\pm0.1$ Once again, as we found previously (figure 11*b*), a notable simplification takes place and all the data points merge onto a single curve. Together with the data of figure 11*b*, we observe that for all lamellar $L_\alpha^C$

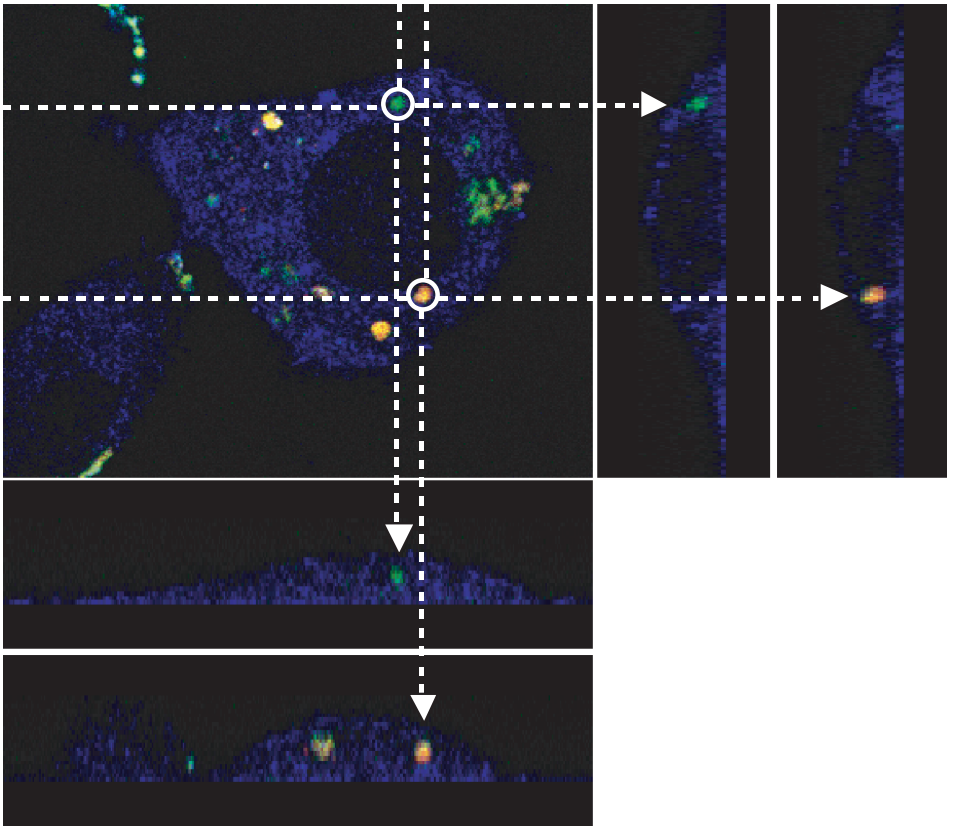

Figure 14. Laser-scanning confocal microscopy image of high-transfecting $L_\alpha^C$ CL–DNA complexes interacting with a mouse fibroblast L-cell, fixed after 6 h (18 wt% DOPC/82 wt% DOTAP, DOTAP/DNA charge ratio = 2.8). DNA is labelled green and lipid is labelled red. In contrast to figure 9 (showing high-transfecting $H_{II}^C$ CL–DNA complexes), no fusion with the plasma membrane is seen implying that the complexes enter cells through endocytosis. Inside the cell, both lipid-free condensed DNA (green) and intact complexes (yellow) are found (both are circled in the $x$–$y$ plane with corresponding arrows in the $x$–$z$ and $y$–$z$ planes). This indicates that if $L_\alpha^C$ complexes are prepared at high charge density ($\sigma_M \approx 0.012$ e Å$^{-2}$, where high TE is observed as shown in figures 11 and 13), they will release DNA inside cells. Adapted from Lin *et al.* (2003).

CL–DNA complexes, $\sigma_M$ is a universal parameter and a predictor of TE. The resulting curve (figure 13) describes a Gaussian $TE = TE_0 + A \exp[(\sigma_M - \sigma_M^*)/w]^2$, with $TE_0 = -(2.4 \pm 0.4) \times 10^7$ RLU mg$^{-1}$ protein, $A = (9.4 \pm 0.6) \times 10^8$ RLU mg$^{-1}$ protein and $w = 5.8 \pm 0.5 \times 10^{-3}$ (e Å$^{-2}$). For the optimal charge density, the fit gives $\sigma_M^* = 17.0 \pm 0.1 \times 10^{-3}$ (e Å$^{-2}$) (Ahmad *et al.* 2005). Significantly, we note that the TE of DOTAP/DOPE containing complexes, which exhibit the $H_{II}^C$ phase in the low $\sigma_M$ region labelled regime I in figure 13, is independent of $\sigma_M$.

Figure 14 shows that the confocal microscopic images of cells interacting with highly transfectant ($\sigma_M \approx 0.012$ e Å$^{-2}$) $L_\alpha^C$ complexes show a completely different path of cell entry and subsequent DNA release than high-transfecting $H_{II}^C$ complexes (figure 9) and low-transfecting $L_\alpha^C$ complexes at low $\sigma_M$ (figure 10, $\sigma_M \approx 0.003$ e Å$^{-2}$). Intact complexes (yellow) were found inside the cell, but more revealing, condensed reporter genes (green-DNA) successfully transferred into

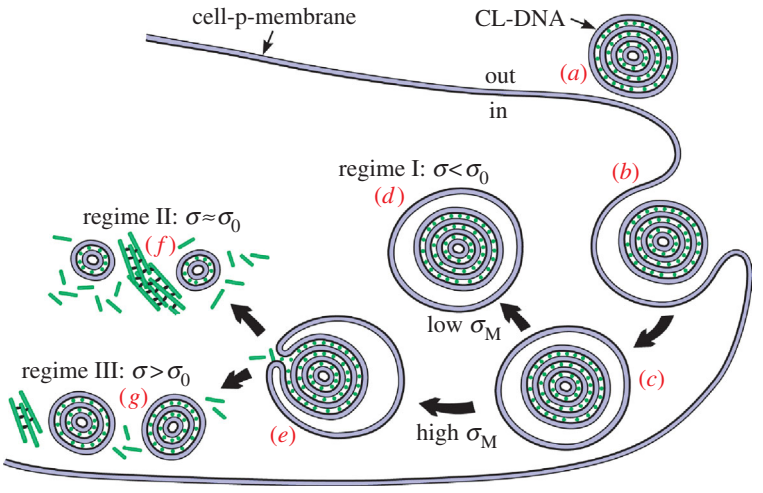


Figure 15. Model of cellular uptake of $L_\alpha^C$ complexes. (*a*) Cationic complexes attach to cells owing to favourable electrostatic interactions and (*b*, *c*) enter through endocytosis. (*d*) Low membrane charge density ($\sigma_M$) complexes remain trapped in endosomes. (*e*) High $\sigma_M$ complexes escape the endosome through fusion. (*f*, *g*) The released smaller complexes are unable to completely dissociate their DNA content (with the effect being more pronounced in regime III at higher $\sigma_M$) and some of the released DNA are further trapped in aggregates with oppositely charged cellular components. Adapted from Ahmad *et al.* (2005).

the cytoplasm are also clearly evident. The image is consistent with the high $\sigma_M$ complexes entering cells through endocytosis. Since endosomes contain no DNA-condensing agent, these condensed aggregates reside in the cytoplasm. The presence of lipid-released DNA in the cytoplasm after endocytic uptake of these complexes implies fusion between CL–DNA lipids and endosomal membranes, which enables escape from the endosomes.

The combined confocal microscopy, enabling visualization of the interactions between complexes and cells, and TE data lead to a model of cellular entry via $L_\alpha^C$ CL carriers (Lin *et al.* 2003; Ahmad *et al.* 2005). The universal TE curve of the lamellar complexes shown in figure 13 may be divided into three well-defined regimes, which correspond to distinct complex–cell interactions (Ahmad *et al.* 2005).

Figure 15 shows a model of cellular uptake of $L_\alpha^C$ complexes. The initial cell attachment is mediated by electrostatics (figure 15*a*) followed by cellular uptake of the complex via endocytosis (figure 15*b*). At low $\sigma_M < \sigma_M^*$ (regime I), where TE increases exponentially with $\sigma_M$ over three orders of magnitude, transfection is limited by endosomal escape (figure 15*c*,*d*) as previously described (figure 11*b* and Lin *et al.* 2003). At high $\sigma_M$, in regimes II and III, complexes are able to overcome this barrier by fusing with the endosomal membrane and releasing smaller complexes into the cytoplasm (figure 15*e*). Different behaviour is observed at $\sigma_M > \sigma_M^*$ in regime III, where TE *decreases* with $\sigma_M$. We hypothesize that transfection is limited by complex dissociation in the cytoplasm owing to the strong electrostatic interaction between the high $\sigma_M$ lipid bilayer and the DNA, and by the release of DNA from aggregates containing cationic cellular components (figure 15*g*), both of which are observed in confocal microscopy (figure 14). The optimal TE in regime II reflects the compromise between

opposing requirements (figure 15*f*): escape from endosomes requires high $\sigma_M$, but dissociation of complexes in the cytoplasm requires low $\sigma_M$. Future strategies for optimization must decouple the opposing requirements.

## 5. Concluding remarks and future studies

We have seen that the membrane charge density ($\sigma_M$) is a universal chemical parameter for transfection by lamellar $L_\alpha^C$ CL–DNA complexes. The newly synthesized series of cationic lipids, with multivalent headgroups, has allowed us to test and verify the generality of the hypothesis concerning $\sigma_M$. Furthermore, we found that the TE of $H_{II}^C$ complexes is independent of $\sigma_M$, with the high TE probably related to the observed rapid fusion (figure 9) between the membranes of complexes containing DOPE and the membranes of the plasma membrane (which might have occurred during endocytosis; Lin *et al.* 2003). One mechanism that may be responsible for the rapid fusion is the fact that the outermost lipid monolayer, which must cover the $H_{II}^C$ complex owing to the hydrophobic effect, is at an opposite curvature to that of the preferred negative curvature of the lipids coating DNA inside the complex (figure 8). This elastically frustrated state of the outer monolayer, which is independent of $\sigma_M$, would then drive rapid fusion with the plasma or endosomal membrane leading to release of a layer of DNA and a smaller $H_{II}^C$ complex within the cell. This process would then repeat itself until all the DNA are released from the complex. By comparison, the bilayers of lamellar $L_\alpha^C$ complexes are inherently more stable and the onion-like (lipid bilayer/DNA monolayer) complex is expected to peel, *layer-by-layer*, much more slowly through interactions of the cationic membranes with anionic components of the cell such as the predominantly anionic actin and microtubule (MT) cytoskeletal filaments (Wong *et al.* 2000; Raviv *et al.* 2005).

The *in vitro* studies described in this paper are expected to be relevant to TE optimization in *ex vivo* cell transfection, where cells are removed and returned to patients after transfection. Our studies, which have a goal of elucidating mechanisms underlying TE in continuous (dividing) cell lines, should aid clinical efforts to develop efficient CL vector cancer vaccines in *ex vivo* applications and possibly *in vivo* applications in local tumours (Rinehart *et al.* 1997; Stopeck *et al.* 1998; Clark & Hersh 1999). The vaccines are intended to induce transient expression of genes coding for immuno-stimulatory proteins in dividing cancer cells, where the nuclear membrane, which dissolves during mitosis, is not considered a barrier to the expression of DNA.

Future experiments, where the bending modulus of the cationic membrane will be varied (Safinya *et al.* 1989), will test the hypothesis that softening of the membrane should enhance TE owing to increased probability of fusion of CL–DNA complexes with endosomal membranes facilitating delivery of complexes into the cytoplasm. In a subtler manner, the Gaussian elastic modulus should also affect TE. To elucidate the role of Gaussian modulus, we intend on studying CL–DNA complexes containing neutral lipids, which by themselves exhibit the bicontinuous cubic phase (membranes with negative surface curvature) owing to a positive Gaussian modulus. As neutral lipids with a negative spontaneous curvature result in the inverse hexagonal $H_{II}^C$ nanostructure, CL–DNA complexes containing membranes with a positive Gaussian modulus should

exhibit a novel bicontinuous cubic lipid–DNA structure. These complexes may show enhanced TE owing to their potential tendency to form energetically favoured pores (with negative curvature) with endosomal membranes releasing DNA into the cytoplasm.

Future experiments will also be conducted using surface-functionalized CL–DNA complexes designed to target cell surface receptors and the nuclear membrane (Jans *et al.* 1998; Cartier & Reszka 2002; Escriou *et al.* 2003; Hebert 2003). This involves using specifically synthesized peptide-spacer lipid molecules with defined peptide sequences and poly(ethylene glycol) spacers of varying lengths. The experiments with peptides containing the RGD (arginine-glycine-aspartic acid) and SV40 nuclear localization sequences (NLS) should serve as models for transfection in slowly or non-dividing cells (which would require the NLS-sequence), and for complexes to be used in systemic *in vivo* delivery applications, where the RGD sequence would attach complexes to RGD-specific surface receptors cells.

### (*a*) *Two state bionanotubes with open and closed ends for gene delivery*

The $H_{II}^{C}$ structure may be viewed as an ordered assembly of nanometre-scale lipid tubules each encapsulating DNA molecules. This raises the question of whether it is possible to develop isolated nanotubes for nucleic acid (genes, gene silencing short interfering RNAs), peptide (Subramanian *et al.* 2000) and chemical delivery applications. This would lead to the unprecedented ability to manipulate the carrier (for example, opening and closing the ends of a tube in response to an external parameter) at the nanometre scale.

The interactions between MTs, which are nanotubes consisting of tubulin polymers derived from the eukaryotic cell with a diameter of the order of 25 nm (Needleman *et al.* 2004*a*,*b*, 2005), and CLs were recently found to result, under the appropriate conditions, in the spontaneous formation of lipid–protein nanotubes (LPNs) with the MT coated by a lipid bilayer under the appropriate conditions (Raviv *et al.* 2005). The LPNs may be viewed as a new paradigm for lipid self-assembly leading to nanotube formation in mixed charged systems, with the MT constituting the oppositely charged anionic macromolecule. It was found that it is possible to switch between two states of the nanotubes, with either open or closed ends with lipid caps, by controlling the cationic lipid/tubulin stoichiometry and the ratio of the macromolecular areas of lipid to MT, $A_{\mathrm{Lipid}}/A_{\mathrm{Microtubule}}$. Thus, the LPNs are model nanotubes for applications involving controlled chemical and gene encapsulation, and release.

Taxol-stabilized MTs were mixed with CLs composed of cationic DOTAP and DOPC as a function of $M^{+}=N_{\mathrm{L}+}/(N_{\mathrm{Lo}}+N_{\mathrm{L}+})$, the mole fraction of cationic lipid ($N_{\mathrm{L}+}$ and $N_{\mathrm{Lo}}$ are the numbers of cationic and neutral lipids, respectively), and $R_{+/-}=N_{\mathrm{L}+}/N_{\mathrm{t}}$, the relative cationic lipid/tubulin stoichiometry ($N_{\mathrm{t}}$ is the number of tubulin dimers with $R_{+/-}=40$ near the isoelectric point of the complex). For $M^{+}>0.1$, the CLs are observed to spread and coat the MT, producing LPN as seen by transmission electron microscopy (TEM) shown in figure 16. At $M^{+}=0.5$, the lipid coverage on the MT is observed to increase as $R_{+/-}$ increases from partial lipid coating at $R_{+/-}=40$ (figure 16*b*, the uncoated part of the MT is clearly visible on the left side) to full coverage at $R_{+/-}=80$ (figure 16*c*). Most interestingly, further increases in $R_{+/-}$ (in the excess CL

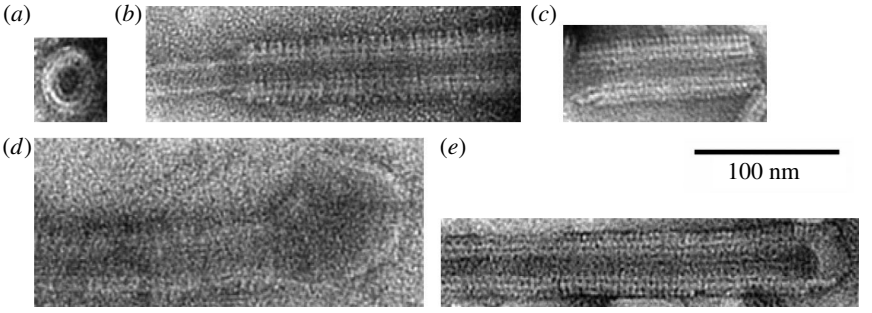


Figure 16. TEM images of the LPNs at different $M^+$ (mole fraction of cationic lipid) and $R_{+/-}=N_{L+}/N_t$ (cationic lipid/tubulin stoichiometric ratio giving the overall charge of the LPN; $R_{+/-}=40$ is the isoelectric point). The LPN spontaneously forms when CLs with $M^+>0.1$ are mixed with microtubules (MTs). (*a*) Cross-section of an LPN. (*b*, *c*) Side views of two LPNs with $M^+=0.5$ and $R_{+/-}=40$, where the partially uncoated MT on the left side in (*b*) is visible, and $M^+=0.5$ and $R_{+/-}=80$, where the MT is fully coated but the ends remain open (*c*). (*d*, *e*) Side views of two LPNs with $M^+=0.5$ and $R_{+/-}=120$ (*d*), and $M^+=0.8$, $R_{+/-}=80$ (*e*), where the LPNs exhibit closed ends consisting of lipid end-caps. The cationic lipid/tubulin stoichiometry and the ratio of the macromolecular areas of the lipid to the microtubule $A_{Lipid}/A_{Microtubule}$ control the open/closed states of the LPN. Adapted from Raviv *et al.* (2005).

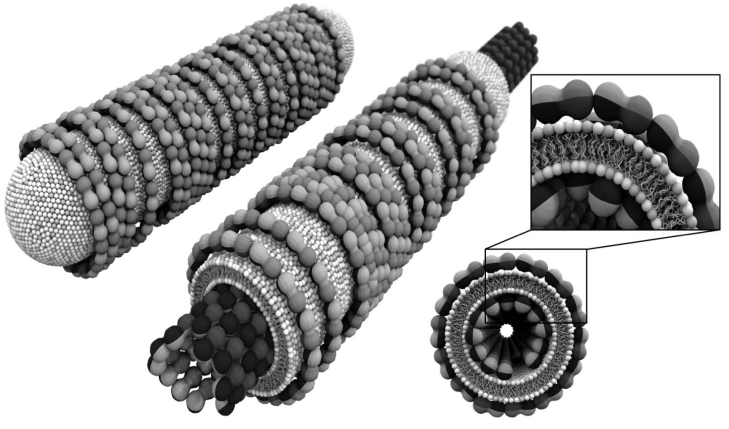

Figure 17. Cartoon of the LPNs with open (middle) and closed ends with lipid caps (left), which form the basis of controlled nanotubes for chemical encapsulation and release as described in the text. Right shows a cross-section and a blow up of the MT–lipid bilayer–tubulin oligomer wall. Redrawn from Raviv *et al.* (2005).

regime) lead to a switch to LPNs with closed ends with lipid caps (figure 16*d*, $R_{+/-}=120$). Figure 16*e* shows another example of an LPN with closed ends at a higher membrane charge density ($M^+=0.8$) for $R_{+/-}=80$.

The TEM images show that the LPN contains an outer third layer (see, the cross-section view of the LPN in figure 16*a*), which is also substantiated in X-ray diffraction experiments (Raviv *et al.* 2005). The rather remarkable architecture of the LPN is shown in the cartoon of figure 17 with the cylindrical lipid bilayer sandwiched between the MT and a controllable partial outer layer of tubulin oligomer. The figure also shows that the LPNs exist in two states and may

contain either open or closed ends with lipid caps, which provides the basis for encapsulation and/or release of chemicals and genes. Using the LPNs in gene delivery applications will require further developments to replace the MT component with a synthetic analogue.

The authors are grateful for the support provided by the US National Institutes of Health grants GM-59288, AI-20611, AI-12520, and the National Science Foundation DMR-0503347.

## References

Ahmad, A., Evans, H., Ewert, K., George, C. X., Samuel, C. E. & Safinya, C. R. 2005 New multivalent lipids reveal bell-curve for transfection versus membrane charge density: lipid-DNA complexes for gene delivery. *J. Genet. Med.* **7**, 739–748.

Bruinsma, R. 1998 Electrostatics of DNA cationic lipid complexes: isoelectric instability. *Eur. Phys. J. B* **4**, 75–88. (doi:10.1007/s100510050353)

Cartier, R. & Reszka, R. 2002 Utilization of synthetic peptides containing nuclear localization signals for nonviral gene transfer systems. *Gene Ther.* **9**, 157–167. (doi:10.1038/sj.gt.3301635)

Cavazzana-Calvo, M. *et al.* 2000 Gene therapy of human severe combined immunodeficiency (SCID)-X1 disease. *Science* **288**, 669–672. (doi:10.1126/science.288.5466.669)

Chesnoy, S. & Huang, L. 2000 Structure and function of lipid-DNA complexes for gene delivery. *Annu. Rev. Biophys. Biomol. Struct.* **29**, 27–47. (doi:10.1146/annurev.biophys.29.1.27)

Clark, P. R. & Hersh, E. M. 1999 Cationic lipid-mediated gene transfer: current concepts. *Curr. Opin. Mol. Ther.* **1**, 158–176.

Edelstein, M. L., Abedi, M. R., Wixon, J. & Edelstein, R. M. 2004 Gene therapy clinical trials worldwide 1989–2004—an overview. *J. Genet. Med.* **6**, 597–602.

Escriou, V., Carriere, M., Scherman, D. & Wils, P. 2003 NLS bioconjugates for targeting therapeutic genes to the nucleus. *Adv. Drug Deliv. Rev.* **55**, 295–306. (doi:10.1016/S0169-409X(02)00184-9)

Ewert, K., Ahmad, A., Evans, H. M., Schmidt, H.-W. & Safinya, C. R. 2002 Efficient synthesis and cell-transfection properties of a new multivalent cationic lipid for nonviral gene delivery. *J. Med. Chem.* **45**, 5023–5029. (doi:10.1021/jm020233w)

Ewert, K., Slack, N. L., Ahmad, A., Evans, H. M., Lin, A. J., Samuel, C. E. & Safinya, C. R. 2004 Cationic lipid-DNA complexes for gene therapy: understanding the relationship between complex structure and gene delivery pathways at the molecular level. *Curr. Med. Chem.* **11**, 133–149. (doi:10.2174/0929867043456160)

Ewert, K., Ahmad, A., Evans, H. M. & Safinya, C. R. 2005*a* Cationic lipid-DNA complexes for non-viral gene therapy: relating supramolecular structures to cellular pathways. *Expert Opin. Biol. Ther.* **5**, 33–53. (doi:10.1517/14712598.5.1.33)

Ewert, K., Ahmad, A., Evans, H. M., Slack, N. L., Lin, A. J., Martin-Herranz, A. & Safinya, C. R. 2005*b* Lipoplex structures and their distinct cellular pathways. In *Non-viral vectors for gene therapy* (ed. L. Huang, M.-C. Hung & E. Wagner), 2nd edn. *Advances in genetics*, vol. 53. San Diego, CA: Elsevier Inc.

Farhood, H., Serbina, N. & Huang, L. 1995 The role of dioleoyl phosphatidylethanolamine in cationic liposome mediated gene transfer. *Biochim. Biophys. Acta* **1235**, 289–295. (doi:10.1016/0005-2736(95)80016-9)

Felgner, P. L. & Rhodes, G. 1991 Gene therapeutics. *Nature* **349**, 351–352. (doi:10.1038/349351a0)

Felgner, P. L., Gadek, T. R., Holm, M., Roman, R., Chan, H. W., Wenz, M., Northrop, J. P., Ringold, G. M. & Danielsen, M. 1987 Lipofection: a highly efficient, lipid-mediated DNA-transfection procedure. *Proc. Natl Acad. Sci. USA* **84**, 7413–7417. (doi:10.1073/pnas.84.21.7413)

Ferber, D. 2001 Gene therapy: safer and virus-free? *Science* **294**, 1638–1642. (doi:10.1126/science.294.5547.1638)

Friedmann, T. 1997 Overcoming the obstacles to gene therapy. *Sci. Am.* **276**, 96–101.

Hacein-Bey-Abina, S. *et al.* 2003*a* A serious adverse event after successful gene therapy for X-linked severe combined immunodeficiency. *N. Engl. J. Med.* **348**, 255–256. (doi:10.1056/NEJM200301163480314)

Hacein-Bey-Abina, S. *et al.* 2003*b* LMO2-associated clonal T cell proliferation in two patients after gene therapy for SCID-X1. *Science* **302**, 415–419. (doi:10.1126/science.1088547)

Harries, D., May, S., Gelbart, W. M. & Ben-Shaul, A. 1998 Structure, stability, and thermodynamics of lamellar DNA-lipid complexes. *Biophys. J.* **75**, 159–173.

Harrington, J. J., Van Bokkelen, G., Mays, R. W., Gustashaw, K. & Williard, H. F. 1997 Formation of de novo centromeres and construction of first-generation human artificial microchromosomes. *Nat. Genet.* **15**, 345–355. (doi:10.1038/ng0497-345)

Hebert, E. 2003 Improvement of exogenous DNA nuclear importation by nuclear localization signal-bearing vectors: a promising way for non-viral gene therapy? *Biol. Cell* **95**, 59–68. (doi:10.1016/S0248-4900(03)00007-8)

Henry, C. M. 2001 Gene delivery—without viruses. *Chem. Eng. News* **79**, 35–41.

Huang, L., Hung, M.-C. & Wagner, E. (eds) 1999 *Non-viral vectors for gene therapy*. San Diego, CA: Academic Press.

Huang, L., Hung, M.-C. & Wagner, E. (eds) 2005 *Non-viral vectors for gene therapy*, 2nd edn. *Advances in genetics*, vol. 53. San Diego, CA: Elsevier Inc.

Hui, S., Langner, M., Zhao, Y., Ross, P., Hurley, E. & Chan, K. 1996 The role of helper lipids in cationic liposome-mediated gene transfer. *Biophys. J.* **71**, 590–599.

Jans, D. A., Chan, C. K. & Hübner, S. 1998 Signals mediating nuclear targeting and their regulation: application in drug delivery. *Med. Res. Rev.* **18**, 189–223. (doi:10.1002/(SICI)1098-1128(199807)18:4<189::AID-MED1>3.0.CO;2-R)

Koltover, I., Salditt, T., Rädler, J. O. & Safinya, C. R. 1998 An inverted hexagonal phase of cationic liposome-DNA complexes related to DNA release and delivery. *Science* **281**, 78–81. (doi:10.1126/science.281.5373.78)

Koltover, I., Salditt, T. & Safinya, C. R. 1999 Phase diagram, stability and overcharging of lamellar cationic lipid–DNA self assembled complexes. *Biophys. J.* **77**, 915–924.

Koltover, I., Wagner, K. & Safinya, C. R. 2000 DNA condensation in two-dimensions. *Proc. Natl Acad. Sci. USA* **97**, 14 046–14 052. (doi:10.1073/pnas.97.26.14046)

Lasic, D. D., Strey, H., Stuart, M. C. A., Podgornik, R. & Frederik, P. M. 1997 The structure of DNA-liposome complexes. *J. Am. Chem. Soc.* **119**, 832–833. (doi:10.1021/ja962713g)

Le Bret, M. & Zimm, B. H. 1984 Distribution of counterions around a cylindrical polyelectrolyte and Manning's condensation theory. *Biopolymers* **23**, 287–312. (doi:10.1002/bip.360230209)

Lin, A. J., Slack, N. L., Ahmad, A., Koltover, I., George, C. X., Samuel, C. E. & Safinya, C. R. 2000 Structure-function studies of lipid-DNA nonviral gene delivery systems. *J. Drug Target.* **8**, 13–27.

Lin, A. J., Slack, N. L., Ahmad, A., George, C. X., Samuel, C. E. & Safinya, C. R. 2003 Three-dimensional imaging of lipid gene-carriers: membrane charge density controls universal transfection behavior in lamellar cationic liposome-DNA complexes. *Biophys. J.* **84**, 3307–3316.

Mahato, R. I. & Kim, S. W. (eds) 2002 *Pharmaceutical perspectives of nucleic acid-based therapeutics*. London, UK: Taylor & Francis.

Manning, G. S. 1978 Limiting laws and counterion condensation in polyelectrolyte solutions. I. Colligative properties. *J. Chem. Phys.* **51**, 924–933. (doi:10.1063/1.1672157)

Marshall, E. 2002 Gene therapy on trial. *Science* **288**, 951–952. (doi:10.1126/science.288.5468.951)

May, S. & Ben-Shaul, A. 2004 Modeling of cationic lipid-DNA complexes. *Curr. Med. Chem.* **11**, 151–167. (doi:10.2174/0929867043456142)

Miller, A. D. 1998 Cationic liposomes for gene therapy. *Angew. Chem. Int. Ed.* **37**, 1768–1785. (doi:10.1002/(SICI)1521-3773(19980803)37:13/14<1768::AID-ANIE1768>3.0.CO;2-4)

Miller, A. D. 2003 The problem with cationic liposome/micelle-based non-viral vector systems for gene therapy. *Curr. Med. Chem.* **10**, 1195–1211. (doi:10.2174/0929867033457485)

Mislick, K. A. & Baldeschwieler, J. D. 1996 Evidence for the role of proteoglycans in cation-mediated gene transfer. *Proc. Natl Acad. Sci. USA* **93**, 12 349–12 354. (doi:10.1073/pnas.93.22.12349)

Mounkes, L. C., Zhong, W., Ciprespalacin, G., Heath, T. D. & Debs, R. J. 1998 Proteoglycans mediate cationic liposome-DNA complex-based gene delivery *in vitro* and *in vivo*. *J. Biol. Chem.* **273**, 26 164–26 170. (doi:10.1074/jbc.273.40.26164)

Nabel, G. *et al.* 1993 Direct gene transfer with DNA-liposome complexes in melanoma: expression, biologic activity, and lack of toxicity in humans. *Proc. Natl Acad. Sci. USA* **90**, 11 307–11 311. (doi:10.1073/pnas.90.23.11307)

Needleman, D. J., Ojeda-Lopez, M., Ewert, K., Jones, J., Miller, H. P., Wilson, L. & Safinya, C. R. 2004*a* Synchrotron X-ray diffraction study of microtubules buckling and bundling under osmotic stress: a probe of inter-protofilament bond strength. *Phys. Rev. Lett.* **93**, 198104-1–198104-4. (doi:10.1103/PhysRevLett.93.198104)

Needleman, D. J., Ojeda-Lopez, M., Raviv, U., Miller, H. P., Wilson, L. & Safinya, C. R. 2004*b* Higher order assembly of microtubules by counter-ions: from hexagonal bundles to living necklaces. *Proc. Natl Acad. Sci. USA* **101**, 16 099–16 103. (doi:10.1073/pnas.0406076101)

Needleman, D. J., Ojeda-Lopez, M., Raviv, U., Ewert, K., Jones, J., Miller, H. P., Wilson, L. & Safinya, C. R. 2005 Radial compression of microtubules by osmotic pressure and the mechanism of action of taxol and microtubule associated proteins. *Biophys. J.* **89**, 3410–3423. (doi:10.1529/biophysj.104.057679)

Niidome, T. & Huang, L. 2002 Gene therapy progress and prospects: nonviral vectors. *Gene Ther.* **9**, 1647–1652. (doi:10.1038/sj.gt.3301923)

Rädler, J. O., Koltover, I., Salditt, T. & Safinya, C. R. 1997 Structure of DNA-cationic liposome complexes: DNA intercalation in multilamellar membranes in distinct interhelical packing regimes. *Science* **275**, 810–814. (doi:10.1126/science.275.5301.810)

Rädler, J. O., Koltover, I., Salditt, T., Jamieson, A. & Safinya, C. R. 1998 Structure and interfacial aspects of self- assembled cationic lipid-DNA gene carrier complexes. *Langmuir* **14**, 4272–4283. (doi:10.1021/la980360o)

Raper, S. E., Chirmule, N., Lee, F. S., Wivel, N. A., Bagg, A., Gao, G. P., Wilson, J. M. & Batshaw, M. L. 2003 Fatal systemic inflammatory response syndrome in a ornithine transcarbamylase deficient patient following adenoviral gene transfer. *Mol. Genet. Metab.* **80**, 148–158. (doi:10.1016/j.ymgme.2003.08.016)

Raviv, U., Needleman, D. J., Li, Y., Miller, H. P., Wilson, L. & Safinya, C. R. 2005 Cationic liposome-microtubule complexes: pathways to the formation of two state lipid-protein nanotubes with open or closed ends. *Proc. Natl Acad. Sci. USA* **102**, 11 167–11 172. (doi:10.1073/pnas.0502183102)

Rinehart, J., Hersh, E., Issell, B., Triozzi, P., Buhles, W. & Neidhart, J. 1997 Phase 1 trial of recombinant human interleukin-1-beta (rhIL-1-beta), carboplatin, and etoposide in patients with solid cancers: southwest oncology group study 8940. *Cancer Invest.* **15**, 403–410.

Roush, W. 1997 Molecular biology: counterfeit chromosomes for humans. *Science* **276**, 38–39. (doi:10.1126/science.276.5309.38)

Safinya, C. R. 2001 Structures of lipid-DNA complexes: supramolecular assembly and gene delivery. *Curr. Opin. Struct. Biol.* **11**, 440–448. (doi:10.1016/S0959-440X(00)00230-X)

Safinya, C. R. (Guest Ed.) 2004 Non-viral vectors for gene therapy and drug delivery. *Curr. Med. Chem.* **11**, 133–220.

Safinya, C. R., Sirota, E. B., Roux, D. & Smith, G. S. 1989 Universality in interacting membranes: the effect of cosurfactants on the interfacial rigidity. *Phys. Rev. Lett.* **62**, 1134–1137. (doi:10.1103/PhysRevLett.62.1134)

Safinya, C. R., Slack, N., Lin, A. & Koltover, I. 2002 Cationic lipid-DNA complexes for gene delivery: structure-function correlations. In *Pharmaceutical perspectives of nucleic acid-based therapeutics* (ed. R. I. Mahato & S. W. Kim), pp. 190–209. London, UK: Taylor & Francis.

Salditt, T., Koltover, I., Rädler, O. & Safinya, C. R. 1997 Two dimensional smectic ordering of linear DNA chains in self-assembled DNA-cationic liposome mixtures. *Phys. Rev. Lett.* **79**, 2582–2585. (doi:10.1103/PhysRevLett.79.2582)

Salditt, T., Koltover, I., Rädler, O. & Safinya, C. R. 1998 Self-assembled DNA-cationic-lipid complexes: two-dimensional smectic ordering, correlations, and interactions. *Phys. Rev. E* **58**, 889–904. (doi:10.1103/PhysRevE.58.889)

Seddon, J. M. 1990 Structure of the inverted hexagonal ($H_{II}$) phase, and non-lamellar phase transitions of lipids. *Biochim. Biophys. Acta* **1031**, 1–69.

Stopeck, A. T., Hersh, E. M., Brailey, J. L., Clark, P. R., Norman, J. & Parker, S. E. 1998 Transfection of primary tumor cells and tumor cell lines with plasmid DNA/lipid complexes. *Cancer Gene Ther.* **5**, 119–126.

Subramanian, G., Hjelm, R. P., Deming, T. J., Smith, G. S., Li, Y. & Safinya, C. R. 2000 Structure of complexes of cationic lipids and poly(glutamic acid) polypeptides: a pinched lamellar phase. *J. Am. Chem. Soc.* **122**, 26–34. (doi:10.1021/ja991905j)

Willard, H. F. 2000 Genomics and gene therapy: artificial chromosomes coming to life. *Science* **290**, 1308–1309. (doi:10.1126/science.290.5495.1308)

Williams, D. A. & Baum, C. 2003 Gene therapy—new challenges ahead. *Science* **302**, 400–401. (doi:10.1126/science.1091258)

Wolff, J. A. (ed.) 1994. *Gene therapeutics: methods and applications of direct gene transfer*. Boston, MA: Birkhäuser.

Wong, G. C. L., Tang, J. X., Lin, A., Li, Y., Janmey, P. A. & Safinya, C. R. 2000 Hierarchical self-assembly of f-actin and cationic lipid complexes: stacked three-layer tubule networks. *Science* **288**, 2035–2039. (doi:10.1126/science.288.5473.2035)

Wrobel, I. & Collins, D. 1995 Fusion of cationic liposomes with mammalian cells occurs after endocytosis. *Biochim. Biophys. Acta* **1235**, 296–304. (doi:10.1016/0005-2736(95)80017-A)

## *Discussion*

A. S. Matharu (*Department of Chemistry, University of York, UK*). How do the cationic liposomes carrying DNA interact or cross cytoskeletal proteins once endocytosis has occurred?

C. R. Safinya. After endocytosis, cationic liposome (CL)–DNA complexes will tend to interact with the oppositely charged biomolecules that they encounter. In particular, positively charged CL–DNA complexes will interact with the cytoskeletal filamentous proteins. These include filamentous-actin, microtubules and intermediate filaments. In fact, the interactions may help to destabilize CL–DNA complexes, which would lead to the release of DNA (a desirable result, since free DNA can be transcribed with the resulting RNA translated into protein).

M.-H. Li (*Institut Curie, France*). Cationic lipids can also form vesicles, where a large volume is available inside. Do you think vesicles would be another good way for gene delivery, using this large volume to encapsulate the DNA?

C. R. Safinya. In fact, nearly 30 years ago, the first synthetic carriers of DNA were either neutral or negatively charged vesicles. These DNA carriers were developed soon after Bangham discovered vesicles. However, such vesicle–DNA complexes are not very efficient in delivering DNA, because all the animal cells are negatively charged and so the electrostatic interactions are not favourable. Hence, researchers switched to cationic liposomes in 1987 to enhance their electrostatic interactions with cells. However, it turns out that under equilibrium conditions, when DNA is mixed with the so-called cationic giant vesicles, the result is the spontaneous formation of self-assembled structures. To date, three structures have been identified unambiguously. These include the lamellar L$\alpha$C phase, with alternating lipid bilayers and DNA monolayers (Rädler *et al.* 1997),

an inverse hexagonal HIIC phase, where DNA is encapsulated within inverse micellar tubules (Koltover *et al.* 1998), and the recently discovered hexagonal HIC phase, where rod-like micelles arranged on a hexagonal lattice are surrounded by DNA, which fills the interstices with honeycomb symmetry (Ewert *et al.* 2006).

V. Percec (*Department of Chemistry, University of Pennsylvania, USA*). You have mentioned that the driving force for the self-assembly of DNA with lipids is provided by the entropy gain provided by the release of counter-ions. Is any molecular weight dependence observed between the molar mass of DNA and the lipid aggregate and the stability of their complex?

C. R. Safinya. I have to assume that the most stable complexes are those prepared near their isoelectric point, where the total number of negative phosphate groups from the DNA backbone equals the cationic groups of the cationic lipid headgroup. This is because the isoelectric point would correspond to the point where most counter-ions are released and hence the entropy gain is maximal. From the isoelectric point of the CL–DNA complex, one may readily determine the ratio of the DNA and cationic lipid molecular weights (and determine, for example, what molecular weight of DNA gives rise to the most stable CL–DNA complex for a given amount of cationic lipid).

J. Seddon (*Department of Chemistry, Imperial College London, UK*). Does the HIIC DNA complex pick up a new outer monolayer from the inner monolayer at the plasma membrane on crossing it into the cytoplasm?

C. R. Safinya. In fact one has to assume that the hydrophobic interaction will require that the HIIC complex always has an outer monolayer (which has a positive curvature). This monolayer can be either from within the complex itself or from the plasma membrane or the endosomal membrane after the complex has interacted with the cell. A thorough discussion of this issue may be found elsewhere (Lin *et al.* 2003; Ewert *et al.* 2005*a*).

## *Additional reference*

Ewert, K. K., Evans, H. M., Zidovska, A., Bouxsein, N. F., Ahmad, A. & Safinya, C. R. 2006 A columnar phase of dendritic lipid-based cationic liposome-DNA complexes for gene delivery: hexagonally ordered cylindrical micelles embedded in a DNA honeycomb lattice. *J. Am. Chem. Soc.* **128**, 3998–4006.